Sound & Vibration 2026, 60(4), 4154.
doi: https://doi.org/10.59400/sv4154

Article

Study on influencing factors of ultrasonic testing for lead seal defects in high-voltage cables

Peng He[*], **Jian Cheng**, **Fengyin Zhang**, **Lianbing Wang**, **Cen Qian**

China Southern Power Grid Shenzhen Power Supply Bureau Co., Ltd., Shenzhen 518000, China

*** Corresponding author:** Peng He, lyc472895899@gmail.com

CITATION

He P, Cheng J, Zhang F, et al. Study on influencing factors of ultrasonic testing for lead seal defects in high-voltage cables. Sound & Vibration. 2026; 60(4): 4154. https://doi.org/10.59400/sv4154

ARTICLE INFO

Received: 13 March 2026
Revised: 10 April 2026
Accepted: 14 April 2026
Available online: 14 July 2026

Abstract: Lead seals are critical sealing and protective components of high-voltage cable terminations, and their structural integrity directly determines the safe and stable operation of urban power transmission systems. Conventional non-destructive testing methods face inherent limitations such as low penetration depth and susceptibility to heat-shrinkable protective layers, making ultrasonic phased array technology a promising alternative for lead-seal defect detection. However, imaging quality is often severely degraded by practical factors encountered in complex field inspection environments. This study systematically investigates the effects of coupling condition, surface roughness, and surface curvature on ultrasonic imaging performance for lead-seal defects. Three groups of controlled comparative experiments were conducted using artificially fabricated lead-seal specimens with predefined internal defects, varying surface roughness levels, and different curvature radii. A dedicated ultrasonic phased array testing platform equipped with a 5 MHz, 16-element probe was established to quantitatively evaluate imaging quality through metrics including signal-to-noise ratio (SNR), contrast-to-noise ratio (CNR), and bottom-wave amplitude. The results show that the improved flexible film coupling device provides significantly better imaging quality than the conventional rigid wedge, with 28.5% higher SNR and 27.8% higher CNR. In addition, increased surface roughness enhances diffuse reflection and reduces echo coherence, while surface curvature introduces spatial phase deviations that weaken bottom-wave response and increase defect interpretation difficulty. These findings provide essential experimental evidence and practical guidance for optimizing field inspection protocols and improving the reliability of ultrasonic testing for high-voltage cable lead seals.

Keywords: cable accessories; lead seals; ultrasonic phased array; defect detection; influencing factors

1. Introduction

With the advancement of urbanization and the continuous growth of power demand, cross-linked polyethylene (XLPE) single-core high-voltage cables are playing an increasingly important role in modern power transmission systems. As a key component of cable accessories, the lead seal serves both protective and sealing functions, and its structural integrity is closely related to the safe and reliable operation of cable terminations. In practical service conditions, defects such as cracks, voids, blowholes, scratches, and deformation may occur due to improper fabrication, external force, or long-term operational vibration. These defects can impair electrical connection and sealing performance and may even lead to severe failures of cable accessories [1].

Therefore, reliable non-destructive testing of lead seals is of considerable engineering importance [2].

At present, several non-destructive methods have been applied to the inspection of lead-seal defects, including loop resistance testing, alternating current field measurement, eddy current testing, and ultrasonic testing [3, 4]. Each method has its own advantages and limitations. For example, electrical methods are often influenced by material conductivity and structural complexity, while eddy current testing is highly sensitive to lift-off distance and has limited capability when thick protective layers such as heat-shrink tubes are present [5–8]. Compared with these methods, ultrasonic testing has advantages in penetration capability, defect localization, inspection efficiency, and practical applicability, and therefore has attracted increasing attention in the inspection of high-voltage cable accessories [9].

Previous studies have demonstrated the feasibility of phased array ultrasonic testing for lead-seal inspection. Techniques such as flexible coupling for curved surfaces, quantitative image-based defect characterization, and multilayer structural positioning have been explored [10–13]. In addition, convolutional neural networks have been applied for automated defect classification, enhancing the potential for precise and rapid evaluation [14]. However, in practical inspection scenarios, phased array ultrasonic imaging of lead seals is still strongly affected by several physical and geometric factors. In particular, unstable coupling conditions, surface roughness, and curved interfaces may alter beam propagation, reduce echo coherence, and degrade image interpretability [15–18].

Accordingly, the present study focuses on the effects of coupling condition, surface roughness, and surface curvature on the ultrasonic imaging performance of lead-seal defects in high-voltage cable accessories [19–22]. By preparing representative lead-seal specimens and establishing an ultrasonic phased array testing platform, comparative experiments were conducted under different surface and coupling conditions, and the corresponding imaging responses were analyzed [23]. The objective of this work is to identify the main factors affecting imaging quality and to provide practical guidance for improving inspection performance in lead-seal applications [24].

It should be noted that, although defect sizing error and discrimination between defect echoes and interface-related echoes are important practical concerns in ultrasonic testing, these issues are not quantitatively resolved in the present study. Instead, this work is limited to the analysis of imaging-quality-related influencing factors. Dedicated quantitative evaluation of sizing accuracy and defect–interface wave separability would require additional ground-truth data and specifically designed validation experiments, and therefore remains a topic for future investigation [25, 26].

2. Test method

2.1. Construction of lead seal defect testing platform

To deeply analyze the effects of lead seal coupling conditions, lead seal surface state, and lead seal defect characteristics on ultrasonic testing results, cable lead seal samples with different roughness, different curvatures, and different defect characteristics were fabricated in this experiment. The defect distribution diagram of the fabricated samples and the appearance of the high-voltage cable accessory lead seal samples are shown in **Figure 1**.

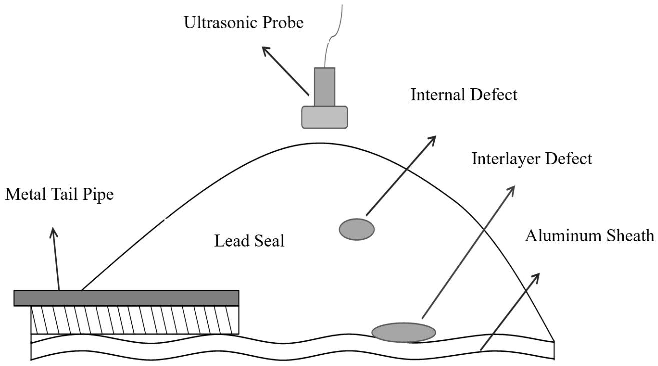

(a) Distribution diagram of fabricated defects on the lead seal.

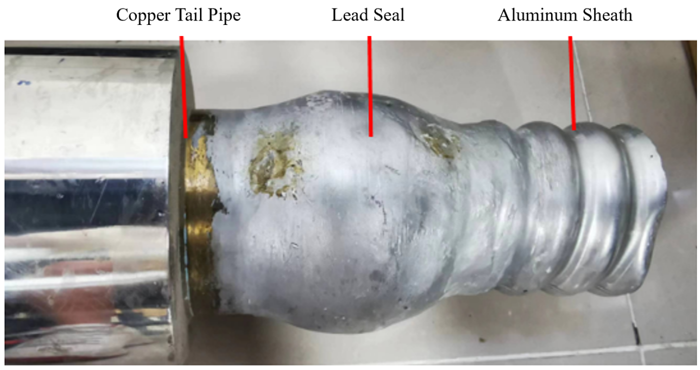

(b) Appearance diagram of high-voltage cable accessory lead seal.

Figure 1. Lead sealing sample of high-voltage cable terminal.

The structure of the ultrasonic testing experimental platform for lead seal defects of high-voltage cable terminations is shown in **Figure 2**. The platform includes ultrasonic phased array testing equipment, probes, couplant, and cable termination lead seal samples. The PA22X ultrasonic phased array instrument produced by Shantou Ultrasonic Electronics Co., Ltd. was used in the experiment.

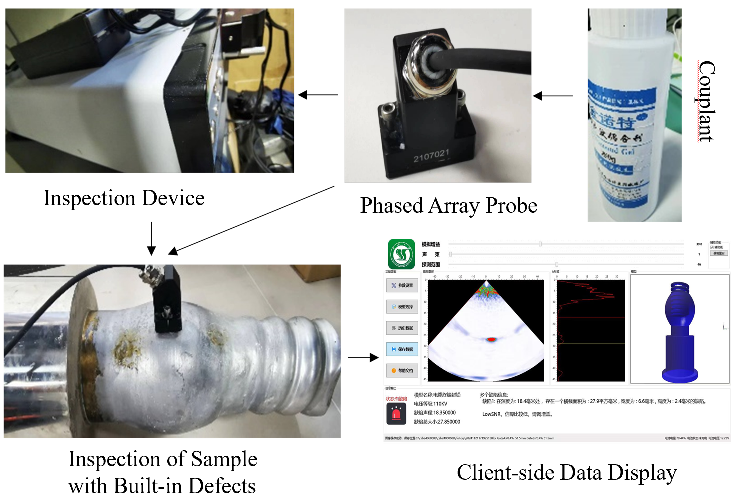

Figure 2. Ultrasonic testing experimental platform of high-voltage cable lead seal defects.

2.2. Analysis of ultrasonic testing results of lead seal defects

During the experiment, the key parameters of the phased array probe were kept constant, including the center frequency of 5 MHz, focal depth of 15 mm, number of elements of 16, element spacing of 0.5 mm, scanning angle of 45°, pulse width set to 200 ns, and detection range set to 40 mm. The basic parameters of the experiments in the following sections are the same as above.

In the sector scan images shown in **Figure 3**, true defect indications are displayed in red. However, a fixed near-surface response region associated with the probe/system, referred to here as the hardware blind area, may also appear in red and should not be misinterpreted as an internal defect. This blind area is mainly located close to the probe-side interface and is related to the early-stage response of the measurement system. In practical interpretation, it can be distinguished from actual defect echoes by the following features: (1) its position is relatively fixed with respect to the probe/interface, (2) it can also be observed in defect-free scans, and (3) it does not exhibit the same spatial distribution or echo morphology as internal defect indications. By contrast, lower-amplitude background responses are displayed in blue.

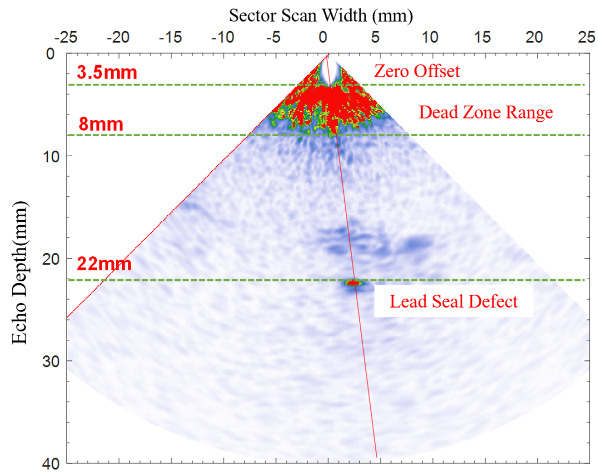

Figure 3. Seal fan scan image defect display information.

Zero offset refers to the reference deviation of time or distance caused by the delay of the probe itself, circuit processing time, or a fixed offset in the sound path during the transmission and reception of ultrasonic waves from the probe. The experimental equipment cannot be calibrated, therefore, when locating the depth of defects, it is necessary to subtract the range of zero offset to obtain the depth information of the defects. For example, the actual depth of the defect in **Figure 3** is 18.5 mm.

3. Analysis of influencing factors on ultrasonic testing of lead seal defects

3.1. Influence of lead seal coupling conditions

3.1.1. Introduction of coupling device

Aiming at the problem of difficult coupling between the ultrasonic probe and the lead seal surface, Fang et al. [1,2,5] designed a flexible coupling device for ultrasonic testing of high-voltage cable lead seals, which can effectively solve the problem of ultrasonic probe energy reception caused by the large surface curvature of high-voltage cable termination lead seals. However, the fixed curvature shape of the designed coupling device cannot adapt to lead seals with multiple curvatures.

Therefore, the coupling structure was further improved in this study, as shown in **Figure 4**. The proposed flexible coupling device mainly consists of an ultrasonic phased array probe, a silicone rubber film, a cylindrical shell, a pressing sheet, and an injection hole. In contrast to the conventional rigid wedge, which has a fixed geometric interface, the present device uses a deformable membrane and an internal couplant-filled cavity to form contact with the inspected surface. The probe is fixed at the upper end of the shell, while the lower end compresses the silicone rubber film through the pressing sheet to achieve sealing and surface conformity. Couplant is injected through the injection hole to expand the membrane and reduce local air gaps at the interface. Under the investigated conditions, this design provides a more adaptive contact state than the rigid wedge when the lead-seal surface deviates from a flat geometry. After completing the above steps, the device can be placed on the lead seal surface for phased array ultrasonic sector detection and ultrasonic data acquisition.

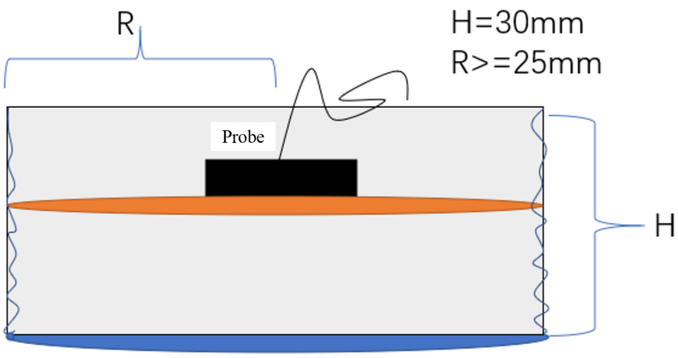

(a) Schematic diagram of the coupling device.

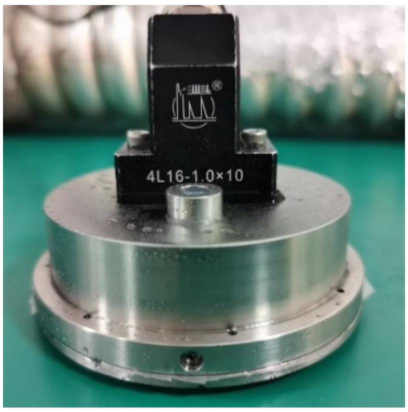

(b) Physical diagram of the coupling device.

Figure 4. Ultrasonic detection coupling device for cable seals.

In this paper, comparative experiments were carried out between the traditional rigid wedge coupling device and the flexible film coupling device to intuitively evaluate the effects of different coupling methods on the phased array ultrasonic imaging performance. As shown in **Figure 5**, under the same detection parameter conditions, the phased array two-dimensional imaging results of the same lead seal sample under two coupling states were obtained, and a comparative analysis was carried out.

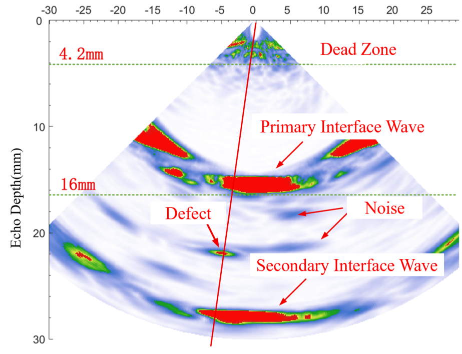

(a) Conventional rigid coupling device.

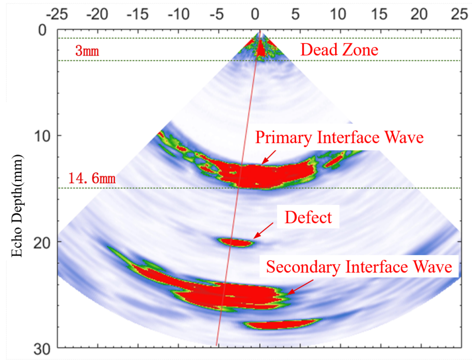

(b) Flexible film coupling device.

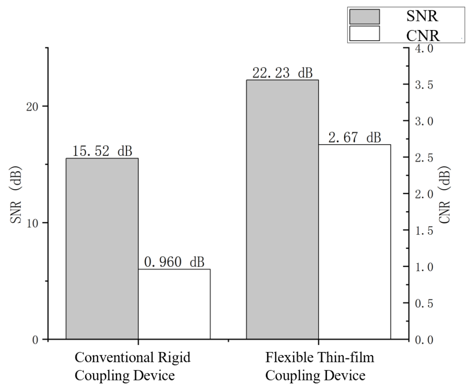

(c) Quantitative comparison between conventional rigid coupling device and flexible film coupling device.

Figure 5. Comparative study of ultrasonic testing results between traditional and flexible coupling devices.

When the traditional rigid wedge is used, although the interface echo information can be obtained, it is difficult for the wedge to achieve stable fitting with the tested surface due to the change of the curvature of the lead seal surface, resulting in the change of the thickness of the coupling layer, which causes the offset of the sound beam incident condition and equivalent sound path, and makes the amplitude of the interface echo fluctuate. The above coupling instability reduces the focusing consistency of the array sound beam, resulting in a low imaging signal-to-noise ratio and a certain degree of geometric distortion.

In contrast, the flexible film coupling device provided more stable surface conformity than the conventional rigid wedge under the tested conditions. The deformable membrane and internal couplant reduced the sensitivity of the coupling state to local surface geometry, which was associated with improved echo continuity and higher SNR/CNR values in the present experiments. The impedance matching medium filled inside reduces the interface reflection loss, and the external flexible structure reduces the influence of coupling condition changes on the sound beam propagation path, so that the continuity and stability of the interface echo and defect echo in imaging are improved. As can be seen from **Figure 5c**, the device is superior to the traditional rigid wedge in both SNR and CNR evaluation indicators, indicating that the flexible film coupling method can effectively improve the imaging quality of phased array ultrasound.

To verify the stability of the test results, as shown in **Table 1**, under eight repeated experiments, flexible film coupling outperformed conventional rigid wedge coupling across all quantitative evaluation metrics. Flexible coupling achieved better results not only in SNR and CNR, which characterize imaging signal quality, but also in PSNR and SSIM, which reflect image fidelity and structural preservation. Meanwhile, the smaller −6 dB mainlobe width indicates better beam focusing and clearer defect boundaries, while the higher DDI further suggests that defect echoes can be more readily distinguished from the background. Overall, these results demonstrate that flexible film coupling not only improves imaging quality but also provides clearer advantages in spatial resolution and defect detectability, indicating better overall inspection performance and greater potential for engineering applications.

Table 1. Statistical results of imaging quality for two coupling methods (n = 8).

Surface condition	SNR/dB	CNR/dB	PSNR/dB	SSIM	−6 dB width/mm	DDI
Smooth Surface	18.42 ± 1.36	18.42 ± 1.36	24.15 ± 1.28	0.71 ± 0.04	2.85 ± 0.21	1.42 ± 0.18
Rough Surface	23.67 ± 0.89	23.67 ± 0.89	29.83 ± 1.12	0.86 ± 0.03	1.92 ± 0.16	2.31 ± 0.22

It should be noted that the statistical results in **Table 1** were obtained from repeated measurements under the current specimen and test configuration and therefore mainly reflect the relative performance difference between the two coupling methods under the investigated conditions. Although the flexible structure is expected to be more suitable for curved surfaces than a rigid wedge, the present study did not include a dedicated quantitative comparison across specimens with multiple known curvature radii. Therefore, the current results should not be interpreted as a complete validation of device performance for all curvature scenarios. More rigorously controlled experiments under multiple curvature conditions are still required in future work.

3.1.2. Experimental testing and analysis

The testing results of the coupling device designed for the curvature of the lead seal in this paper are shown in **Figure 6**. When in the non-testing state, the primary and secondary waves of the film interface can be clearly seen; when placed on the lead seal surface without internal defects, the primary waveform of the coupling interface is relatively complete, but the secondary wave is seriously deformed, and the lead seal bottom wave appears between the primary and secondary waves. This is because the probe with coupling can achieve better coupling with the lead seal with curvature, receive higher energy, and can better detect defects. But at the same time, additional noise and interface-related echoes are introduced, which increase interpretation uncertainty. Under the present experimental conditions, defect location could still be identified, whereas further quantitative characterization of defect geometry was less reliable. However, the coupling device may improve the visibility of near-surface echoes originally located in the blind-zone-affected region; however, this observation was mainly based on image comparison, and a dedicated quantitative evaluation of blind-zone reduction was not performed in the present study. The reason is that the coupling device changes the original imaging area under the probe blind area to between the primary interface and secondary interface waves, which helps the detection of near-surface defects to a certain extent.

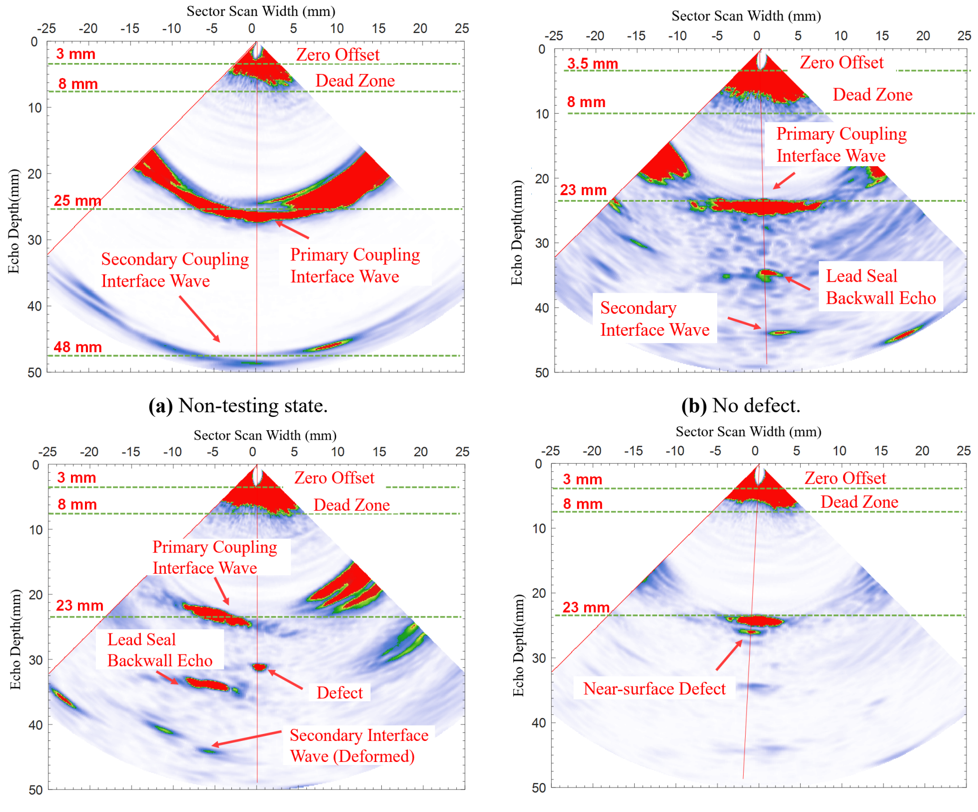

(a) Non-testing state. **(b)** No defect. **(c)** Internal defect. **(d)** Near-surface defect.

Figure 6. Ultrasonic detection results of the lead seal coupling device.

However, the coupling device may improve the visibility of near-surface echoes originally affected by the probe blind area. A possible reason is that the coupling structure shifts the effective imaging region from the original blind-area-affected zone to the region between the primary and secondary interface waves. It should be noted, however, that this observation is based mainly on qualitative image comparison in the present study, and no dedicated quantitative evaluation of blind-zone reduction or minimum detectable near-surface depth was performed. Therefore, this effect should be interpreted as a preliminary observation rather than a fully validated quantitative conclusion.

Future work should include dedicated experiments using near-surface reference reflectors or blind-zone depth measurements to quantitatively evaluate whether the coupling device improves the detectability of near-surface defects.

To further verify the effectiveness of the coupling device, comparative testing experiments were continued on lead blocks and lead seals, as shown in **Figure 7a,b**. Lead block and lead seal samples were prepared respectively in the experiment, and the specific defect information is shown in **Figure 7c,d**.

The testing results are shown in **Figure 8**. The testing effect is good when detecting lead blocks, and multiple defects can be detected. Because when ultrasonic waves pass through the glycerol medium and the flat lead block, the ultrasonic refraction angle is small, the ultrasonic probe receives good signals, and the focusing law of the ultrasonic equipment is suitable for flat surface detection. However, compared with the flat lead block, the curved lead-seal specimen showed reduced image clarity and lower interpretability of defect echoes under the same inspection settings. This reduction is attributed to the mismatch between the actual curved propagation path and the delay law designed for flat-surface focusing, which increases positioning uncertainty and limits achievable detection accuracy under conventional inspection conditions.

(a) Lead block.

(b) Lead seal.

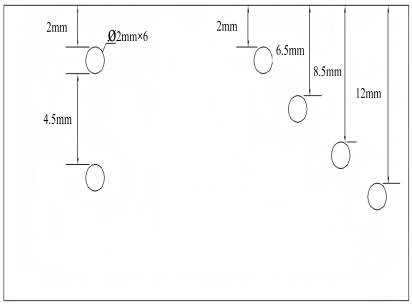

(c) Detailed defect information of lead block sample.

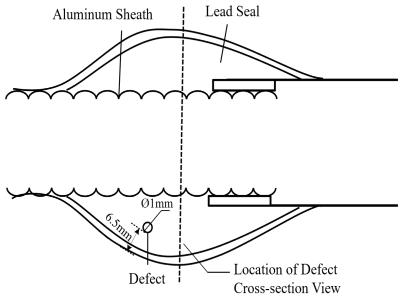

(d) Detailed defect information of lead seal sample.

Figure 7. Coupling device detection of lead blocks and seals.

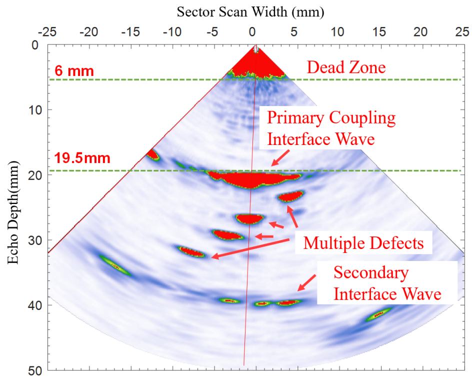

(a) Testing result of the lead block.

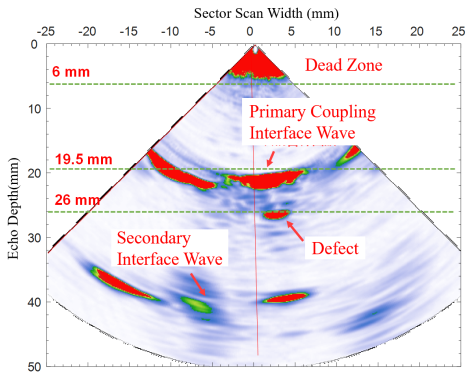

(b) Testing result of the lead seal.

Figure 8. Test results of the coupling device of the lead block and the lead seal.

Therefore, the present results mainly demonstrate the relative advantage of the flexible coupling design under the investigated conditions, while its quantitative performance across multiple curvature scenarios still requires further controlled validation. In the actual application process, the coupling device can be applied for auxiliary testing according to the actual situation.

3.2. Influence of lead seal surface roughness

3.2.1. Analysis of the influence mechanism

In phased array ultrasonic testing, the propagation behavior of ultrasonic waves on the surface of the test piece has a decisive influence on the imaging quality. Ideally, ultrasonic waves mainly undergo specular reflection and regular refraction at the smooth interface; the sound beam energy is concentrated, and the wavefront maintains good coherence. When the tested surface has a certain roughness, the random fluctuation of the interface morphology will significantly change the propagation characteristics of ultrasonic waves, thereby adversely affecting the imaging signal-to-noise ratio and defect identifiability.

(1) Influence of a rough interface on ultrasonic reflection and scattering behavior

From the perspective of acoustic theory, surface roughness can be characterized by the relative relationship between its root mean square height σ and ultrasonic wavelength λ. When the interface roughness satisfies: $\sigma \ll \frac{\lambda}{8}$, the interface can be approximately regarded as a smooth interface, and ultrasonic waves mainly undergo specular reflection. The reflected sound pressure amplitude can be expressed as:

$$p_r = R \cdot p_i. \tag{1}$$

Where p_i is the incident sound pressure, and R is the reflection coefficient, which is related to the acoustic impedance of the material. However, when the roughness increases gradually, the interface can no longer be regarded as an ideal plane, and significant diffuse reflection and scattering of ultrasonic waves will occur at the interface. When single scattering occurs on a surface whose local curvature radius is much larger than the ultrasonic wavelength, and the surface height distribution follows an isotropic Gaussian random stationary process, the incident sound energy is redistributed to multiple directions, and its scattering intensity can be approximately described by the classical rough interface scattering model as:

$$I_s(\theta) \propto I_0 \exp\left[-\left(\frac{4\pi\sigma\cos\theta}{\lambda}\right)^2\right]. \tag{2}$$

Where I_s is the scattered sound intensity, θ is the scattering angle, and I_0 is the incident sound intensity. It can be seen that the increase in roughness σ will lead to significant attenuation of effective reflected sound energy, thereby weakening the effective echo signal returned to the probe.

(2) Influence of roughness on coherence and focusing performance of phased array sound beams

Phased array ultrasonic testing relies on precise phase control between elements to form sound beam convergence in the target area. For an ideal smooth interface, the sound waves emitted by different elements maintain high phase consistency during propagation, and the wavefront can be approximately expressed as:

$$p(r,t) = A(r)\cos(\omega t - k \cdot r). \tag{3}$$

Where k is the wave vector. Under the condition of a rough interface, the interface fluctuation will introduce additional random phase perturbation $\Delta\phi(r)$, making the wavefront evolve into:

$$p(r,t) = A(r)\cos[\omega t - k \cdot r + \Delta\phi(r)]. \quad (4)$$

These random phase perturbations will destroy the coherent superposition condition between elements, resulting in the decrease of sound beam main lobe energy and the enhancement of side lobes, thus reducing the sound pressure amplitude in the focal area and diffusing the energy distribution. This phenomenon is manifested as the weakening of defect echo amplitude, discontinuous bottom waves, and enhanced background noise in phased array sector scan imaging. Theoretical analysis shows that the relative ratio of interface roughness to acoustic wavelength is the core factor determining the coherence of the sound beam. When σ is close to or exceeds the wavelength, the energy loss and random phase perturbation caused by diffuse reflection will directly lead to the degradation of imaging quality.

It should be noted that the above scattering and phase-perturbation expressions are derived under simplified assumptions, including the single-scattering approximation, idealized random roughness distribution, and relatively simple interface conditions. In actual lead seals, however, the surface morphology may deviate from an ideal Gaussian-type rough surface, and local air gaps, multilayer interfaces, material inhomogeneity, and irregular geometric features may coexist. Under such conditions, the actual ultrasonic propagation behavior can be more complicated than that described by the simplified model. Therefore, the above analytical expressions are mainly used to explain the qualitative trend that increasing roughness degrades beam coherence and imaging quality, rather than to provide an exact quantitative prediction of echo attenuation or image degradation in real lead-seal structures.

3.2.2. Analysis of simulation results

To deeply analyze the influence of surface morphology on the evolution characteristics of ultrasonic phased array sound beams, this paper constructs a two-dimensional transient acoustic numerical simulation model using COMSOL Multiphysics software. To ensure that the simulation results have reliable engineering guidance value, the physical parameters of the lead seal matrix, internal aluminum sheath, and coupling medium layer (water) in the model are strictly set with reference to the test pieces used in the experiment. The detailed mechanical and acoustic transmission parameters are shown in **Table 2**.

Table 2. Ultrasonic transmission parameters.

Material	Sound velocity/($m \cdot s^{-1}$)	Density/($g \cdot cm^{-3}$)	Acoustic impedance/($g \cdot cm^{-2} \cdot s^{-1}$)
Lead	2,200	11.34	2.46×10^6
Aluminum	6,300	2.7	1.7×10^6
Air	340	1.29×10^{-3}	0.00004×10^6
Water	1,500	1	0.15×10^6

In the wave field evolution simulation, the internal defects are equivalent to air medium filling. Due to the significant difference in acoustic impedance between air and the lead seal matrix, the interface sound pressure reflection coefficient R is close to -1, which ensures that the incident sound wave is almost totally reflected at the defect position, thus accurately restoring the scattering characteristics of the defect. In contrast, the reflection coefficient of the interface between the lead seal and the aluminum sheath is small (R ≈ 0.18), which ensures that the sound beam has good transmission characteristics at the heterogeneous interface and conforms to the propagation logic of the bottom-wave signal under actual working conditions.

To accurately restore the scattering effect of defects on the sound beam, the defect interface is defined as a free boundary. Except for the area where the excitation source element is located, the peripheral boundary of the model is set as a low reflection boundary to effectively absorb outgoing traveling waves and prevent the artifact echo generated by the artificial truncated boundary from interfering with the analysis results. In addition, to meet the requirements of calculation convergence and accuracy, the model meshing follows the criterion that the element size is less than 1/6 of the acoustic wavelength, and the time step is set according to the CFL condition.

In the present wave-field simulation, the internal defect is idealized as an air-filled cavity. This simplified representation is mainly used to reproduce the strong acoustic-impedance mismatch between the defect region and the lead matrix, so that the basic reflection and scattering trend of a strong discontinuity can be observed. However, it should be noted that actual lead-seal defects may include cracks, pores, scratches, or interfacial flaws whose geometries and scattering behaviors are not fully equivalent to those of an air-filled cavity. Therefore, the present defect model should be regarded as an idealized approximation for qualitative analysis, rather than a complete physical reconstruction of all realistic defect types in lead seals.

Consequently, the purpose of the current COMSOL model is to compare the relative difference in wave-field evolution under smooth and rough surface conditions, instead of quantitatively reproducing the echo response of every specific defect morphology encountered in practical lead-seal inspection.

In this paper, the time-domain simulation model of lead seal defects is established by using the acoustic-structure coupling interface in COMSOL. To truly simulate the sound field characteristics of the phased array probe, the sinusoidal pulse modulated by the Hanning window is used as the excitation signal of each element, and its expression is shown in formula (5). Where f_0 is the frequency of the excitation signal, T_0 is the period, and D_i is the delay time of the *i*-th wafer. By applying a specific time delay D_i to each wafer, the deflection and focusing control of the ultrasonic beam are realized as shown in the figure. The application of the window function can effectively suppress spectrum leakage and high-frequency interference, making the characteristics of the excitation source closer to the actual detection working conditions.

$$f(t) = 100 \exp\left(-\left(\frac{t-(T_0-D_i)}{\frac{T_0}{2}}\right)^2\right) \times \sin\left(2\pi f_0 \times (t-D_i)\right). \tag{5}$$

The ultrasonic excitation signal applied to the elements is shown in **Figure 9**. By applying different time delays to the excitation signal of each element, the deflection and focusing of the ultrasonic beam can be realized.

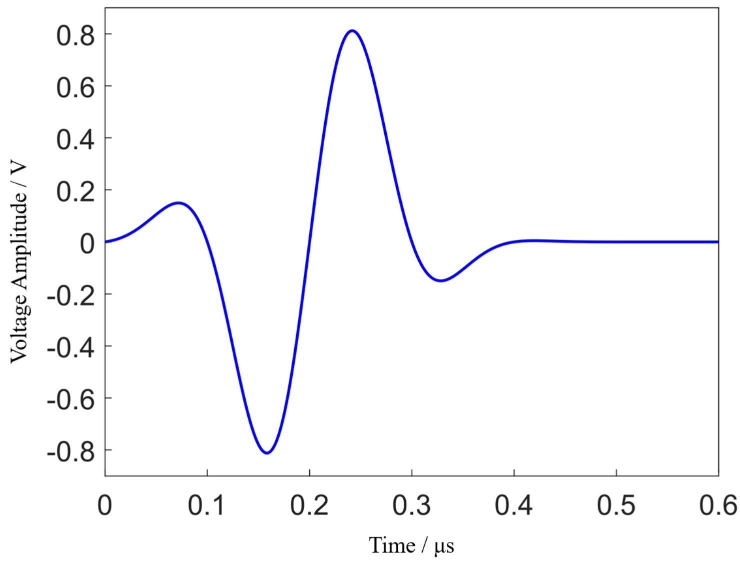

Figure 9. Ultrasonic excitation signal.

Under the condition of consistent excitation mode, element arrangement, and material parameters, the sound pressure field distributions of the two models at the same time were compared and analyzed. The following results are all based on transient sound field snapshots to intuitively reveal the differences in sound beam propagation trajectories and wavefront evolution characteristics.

(1) Sound field propagation characteristics under smooth surface condition

Figure 10 shows the two-dimensional total sound pressure snapshot obtained by the phased array probe exciting the smooth surface of the cable lead seal at the transient time t = 5 × 10^{-7} s. Several significant characteristics representing the smooth interface can be seen from the figure: first, the color mapping presents a continuous and gentle transition from positive pressure to negative pressure, and the color gradient change of the whole sound field is uniform without obvious pixelation and point mutation; second, the superimposed isobars are regular arcs and concentric closed curves, with stable intervals, smooth outlines, and strong ductility, without local fracture or highly irregular isobaric bifurcation caused by rough or discontinuous geometry.

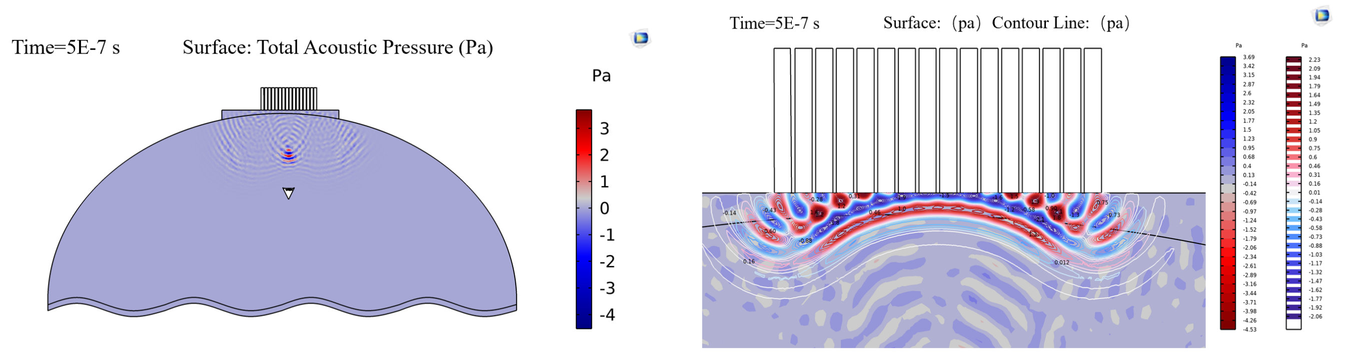

(a) Overall sound pressure diagram of a lead seal with a smooth surface.

(b) Local sound pressure distribution diagram of the smooth surface of the lead seal.

Figure 10. Simulation of transient acoustic field for lead sealing with a smooth surface.

Further observation of the sound pressure distribution shows that the main lobe area of the sound beam has a high sound pressure amplitude, a high degree of energy concentration, and the wavefront shape remains stable during propagation. This regular wavefront evolution is conducive to the coherent superposition of sound waves between elements, so that the phased array sound beam can form a clear convergence trend in the target area, thus providing good propagation conditions for the formation of subsequent defect echoes.

(2) Sound field propagation characteristics under rough surface conditions

In contrast, after the introduction of surface roughness, the sound field snapshot presents significantly different propagation characteristics. **Figure 11** shows the obtained two-dimensional total sound pressure distribution nephogram when the phased array probe acts on the rough surface of the cable lead seal at the transient time t $= 5 \times 10^{-7}$ s. Near the rough interface, the original continuous wavefront structure is destroyed, and the isobars show local distortion and irregular splitting. This indicates that the ultrasonic wave has significant multi-directional scattering at the rough interface, and the incident sound energy is redistributed to different propagation directions.

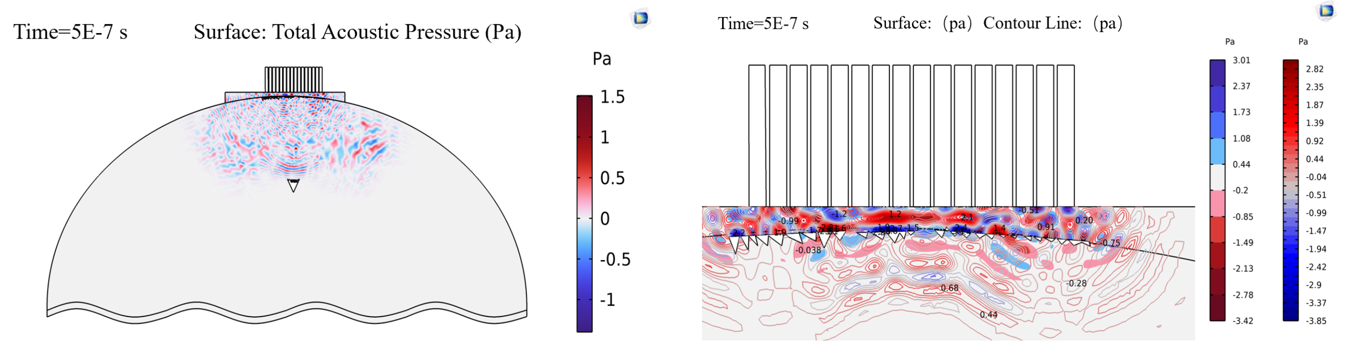

(a) Overall sound pressure diagram of a lead seal with a rough surface.

(b) Local sound pressure distribution diagram of the rough surface of the lead seal.

Figure 11. Simulation of transient acoustic field for lead sealing with rough surface.

Based on the high irregularity of isobars, the large fluctuation of local sound pressure values on a very short spatial scale and the numerical characteristics of significantly increased peak-to-peak value, it can be clearly judged that the lead seal surface shows typical acoustic rough interface characteristics under the current wavelength scale. The rough structure significantly enhances the multi-path propagation and local interference effect of sound waves, leading to the redistribution of sound field energy and the generation of a large number of high spatial frequency components, thus weakening the coherent focusing ability of the phased array sound beam.

The above numerical comparison shows that surface roughness can noticeably alter wavefront continuity, beam directivity, and local sound-field distribution. Under the present modeling assumptions, the simulation results provide qualitative support for understanding how rough surfaces may enhance scattering and weaken coherent focusing. However, since the current model uses an idealized defect representation and no quantitative indicators such as SNR or matched echo amplitude were extracted for direct comparison with experiments, the simulation in this section should be interpreted as a qualitative illustration rather than a fully validated quantitative mechanistic model. More rigorous validation will require future simulations using defect geometries closer to actual cracks or pores, together with the extraction of comparable quantitative metrics within matched observation windows.

It should also be emphasized that the current simulation was not intended to establish a one-to-one quantitative correspondence with the experimental results. In particular, quantitative quantities such as SNR, echo peak amplitude, or echo energy were not extracted from the simulated signals and compared directly with the experimental measurements. Therefore, the role of the present simulation is mainly to illustrate the physical trend of sound-field distortion and scattering evolution caused by surface roughness, while the experimental results remain the primary basis for quantitative performance evaluation in this study.

3.2.3. Experimental testing and analysis

In the production process of high-voltage cable lead seals, improper lead pouring technology will cause rough lead seal surface due to manual influence. Due to the contact detection characteristic of ultrasonic phased array, when the convex scale of the lead seal surface is close to or larger than the ultrasonic wavelength, Rayleigh scattering and diffuse reflection will be caused. If the rough surface forms microscopic air gaps, it will lead to discontinuous acoustic impedance, thus refracting the sound beam, which seriously affects the propagation and reception of ultrasound.

In this section, aiming at the roughness problems that may be encountered in lead seals in actual technology, samples from smooth ($Ra \approx 1.6$ μm $\ll \lambda$) to rough (simulating obvious bulges formed by improper manual lead pouring technology in practice, $\sigma \approx \lambda$) were fabricated as shown in **Figure 12**, to quantitatively verify the signal-to-noise ratio attenuation law caused by roughness and guide the necessity evaluation of lead seal surface pretreatment in the engineering field. Among them, the lead seal without a heat-shrinkable tube simulates the lead seal technology level before actual operation, and the lead seal sample with a heat-shrinkable tube simulates the lead seal in actual operation.

(a) Rough surface. **(b)** Smooth surface. **(c)** Wrapped with heat-shrinkable tube.

Figure 12. Samples of seals with different roughness.

In this paper, comparative ultrasonic phased array testing experiments were carried out on lead seal specimens with different surface states. The testing results are shown in **Figure 13a–f**, and the experimental phenomena highly confirm the scattering model and phase distortion theory described in Subsection 2.2.1.

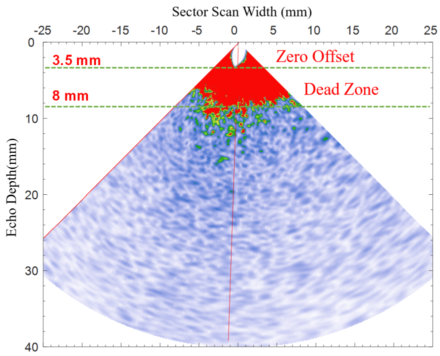

(a) Rough surface without defect.

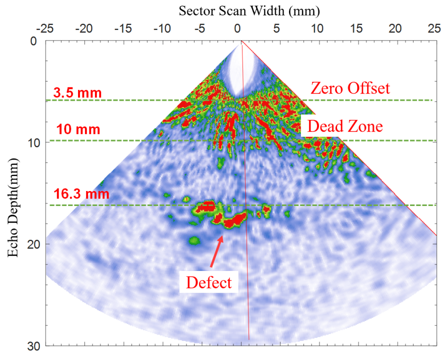

(b) Rough surface with defect.

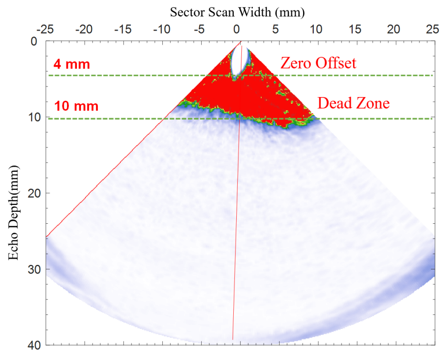

(c) Smooth surface without defect.

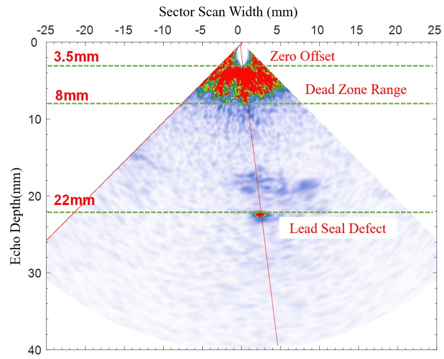

(d) Smooth surface with defect.

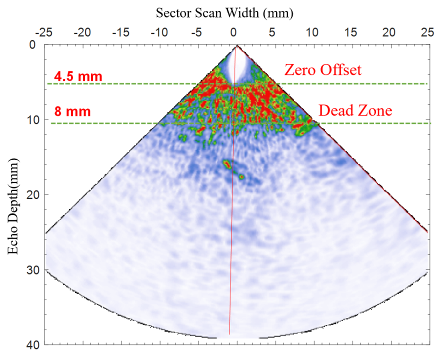

(e) Lead seal with heat-shrinkable tube without defect.

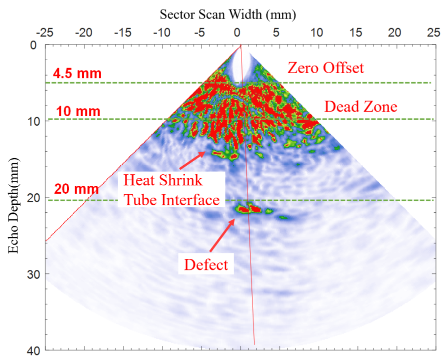

(f) Lead seal with heat-shrinkable tube with defect.

Figure 13. Seal detection results of different roughness.

First of all, by comparing **Figure 13a**,**b**, it can be observed that the lead seal with a rough surface has a lot of background noise even when no defect is detected, and the defect echo signal is weak. The physical mechanism behind this phenomenon is: due to the large root mean square height σ of the rough surface, the incident sound energy undergoes intense spatial diffuse reflection according to formula (2), resulting in significant attenuation of the effective coherent energy I_s that can return to the probe along the original path. At the same time, the random fluctuation of the lead seal surface introduces additional phase perturbation $\Delta\phi$ for each element, which destroys the coherent superposition and focusing conditions of the phased array sound beam, leading to the decrease of the main lobe energy of the sound beam and the enhancement of the side lobes, which is manifested as a significant increase in background noise in the image.

Secondly, for the lead seal samples coated with heat-shrinkable tube (**Figure 13e**,**f**), the experimental results show that the blind-zone-affected region became larger, and the echo pattern became more complex. This is because the heat-shrinkable tube introduces an additional multi-layer acoustic interface, and strong interface reflection and acoustic impedance mismatch occur when the sound wave passes through the tiny air gap between the heat-shrinkable tube and the lead seal, further consuming the sound energy transmitted into the lead seal. Although internal defects can still be identified, as a result, quantitative interpretation of defects became less reliable under this condition. due to the sound attenuation caused by the heat-shrinkable tube and the interference of multiple reflected echoes.

In summary, the experimental data verify the prediction about the destruction of sound beam coherence in the theoretical derivation: the rougher the surface and the closer the ratio of acoustic wavelength to roughness, the more serious the energy loss and phase perturbation caused by diffuse reflection. Therefore, for lead seals with smooth surfaces and no heat-shrinkable tubes, the sound beam maintains good directivity and coherence; the smooth-surface condition provided the highest image quality among the tested surface conditions. While the working conditions with rough surfaces and heat-shrinkable tubes limit the quantitative accuracy of ultrasonic testing due to the sound field distortion at the physical mechanism level.

It should be noted that the heat-shrink tube condition does not represent a pure roughness change alone, because the additional multilayer interface and possible microscopic air gaps may also affect ultrasonic propagation and echo characteristics.

The comparison results of SNR and CNR between **Figure 13b**,**d** are shown in **Figure 14**.

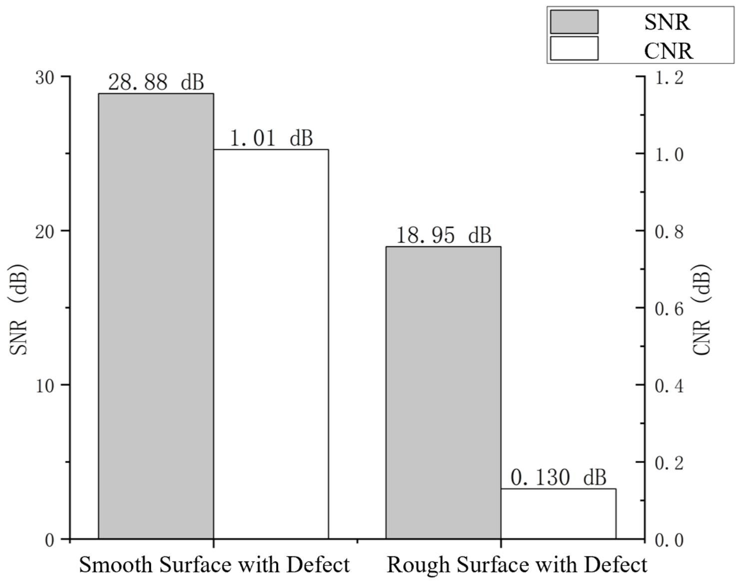

Figure 14. SNR and CNR corresponding to the detection of lead seals with different roughness levels.

As shown in **Table 3**, under eight repeated experiments, the smooth surface condition outperformed the rough surface condition across all quantitative evaluation metrics. In addition to the originally reported SNR and CNR, the smooth surface also showed better PSNR and SSIM values, indicating improved image quality and structural preservation. Meanwhile, the smaller −6 dB mainlobe width under the smooth surface condition suggests more concentrated beam focusing and clearer defect boundaries, while the higher DDI indicates that defect echoes can be more readily distinguished from the background. Overall, the increase in surface roughness leads to a simultaneous degradation in imaging quality, spatial resolution, and defect detectability, whereas the smooth surface condition provides more stable detection results and clearer images, which are more favorable for defect identification and interpretation.

Table 3. Statistical results of imaging quality under different surface conditions (n = 8).

Surface condition	SNR/dB	CNR/dB	PSNR/dB	SSIM	−6 dB width/mm	DDI
Smooth Surface	28.74 ± 0.92	1.03 ± 0.08	33.21 ± 1.05	0.91 ± 0.02	1.68 ± 0.14	2.74 ± 0.19
Rough Surface	19.12 ± 1.15	0.15 ± 0.06	24.86 ± 1.27	0.73 ± 0.04	2.97 ± 0.22	1.36 ± 0.17

3.3. Influence of lead seal surface curvature

3.3.1. Analysis of the influence mechanism

(1) Surface geometry and local normal deviation

Establish a coordinate axis x in the transverse direction of the array, and describe the geometric morphology of the lead seal surface with the height function $h(x)$. For a curved surface with a local approximate arc, its height function is expressed as:

$$h(x) = R - \sqrt{R^2 - x^2}. \tag{6}$$

Where R is the radius of curvature. The local normal deviation angle $\varphi(x)$ of the curved surface at position x is defined as the deflection angle of the normal at this point relative to the global reference normal:

$$\varphi(x) = \text{arctan}\left(\frac{\mathrm{d}h(x)}{\mathrm{d}x}\right). \tag{7}$$

Under the condition of small slope $|dh/dx| \ll 1$, the first-order approximation can be adopted. This relationship shows that the sound waves at different transverse positions of the array will enter the workpiece at different local incident angles, and the angle deviation increases significantly with the decrease of the curvature radius. It leads to different local normals at each element, and directly changes the effective incident angle of each element to the same spatial point.

$$\varphi(x) \sim \frac{\mathrm{d}h(x)}{\mathrm{d}x} \sim \frac{x}{R}. \tag{8}$$

(2) Deterministic calculation of path difference and phase distortion

In the design of phased array focusing, it is usually assumed that the tested surface is a plane, and the element delay is calculated accordingly, so that the sound waves of each element achieve consistent phase at the predetermined focal point (xf, yf). If the plane assumption is still adopted, the reference propagation path length from the x-th element to the focal point is:

$$L_0(x) = \sqrt{(x - x_f)^2 + (0 - y_f)^2}. \tag{9}$$

When the actual surface is a curved surface, the sound wave propagates from the curved surface point (*x, h(x)*) to the focal point, and its real propagation path length is:

$$L(x) = \sqrt{(x - x_f)^2 + (h(x) - y_f)^2}. \tag{10}$$

The geometric path difference introduced therefrom is:

$$\Delta L(x) = L(x) - L_0(x). \tag{11}$$

Under the condition of small curvature, the above formula can be approximated as:

$$\Delta L(x) \approx \frac{x^2}{2R}. \tag{12}$$

It shows that the path difference presents a quadratic distribution in the array range. The path difference is further transformed into phase distortion, and its expression is:

$$\Delta\phi(x) = \frac{2\pi}{\lambda}\Delta L(x). \tag{13}$$

Where λ is the wavelength of the ultrasonic wave in the medium. It can be seen that even under the premise of a completely correct delay law, curvature will inevitably introduce spatially related phase errors. The specific schematic diagram is shown as follows (**Figure 15**):

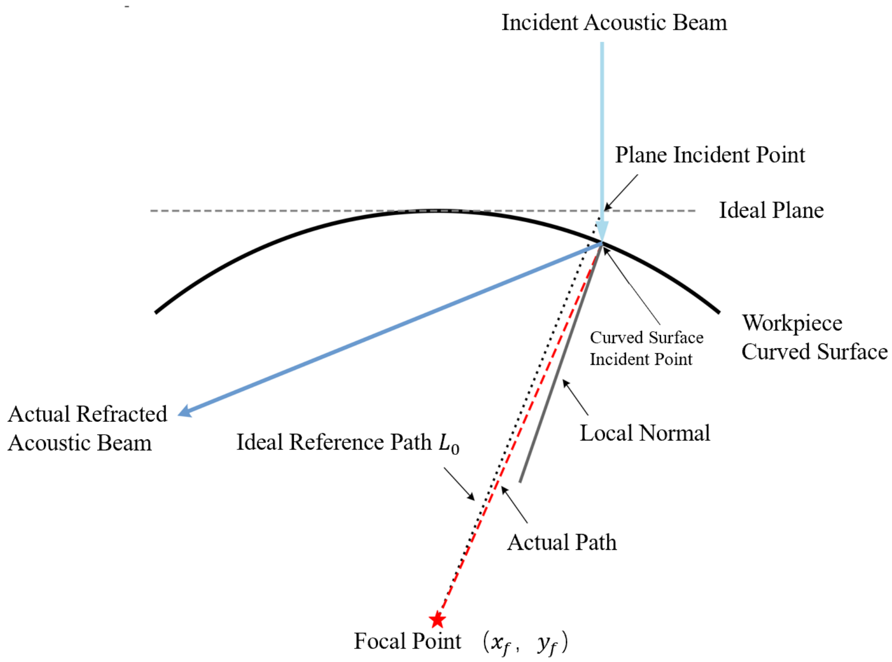

Figure 15. The effect of curvature on the ultrasonic propagation path.

(3) Influence of phase distortion on array coherent superposition

At the focal plane, the complex amplitude contributed by the n-th element can be expressed as:

$$E_n(r) = A_n \exp\left[i\left(\phi_n^{(0)} + \Delta\phi\left(x_n\right)\right)\right]. \tag{14}$$

Where $\phi_n^{(0)}$ is the phase term under ideal plane conditions, and $\Delta\phi\left(x_n\right)$ is the additional phase distortion caused by curvature. The total field of the array is the vector sum of the complex amplitudes of each element:

$$E(r) = \sum\nolimits_{n=1}^{N} E_n(r). \tag{15}$$

When $\Delta\phi\left(x_n\right) = 0$ the elements achieve complete in-phase superposition at the focal point, forming an ideal focused sound field with high amplitude and a narrow main lobe. On the contrary, when $\Delta\phi\left(x_n\right)$ changes with the position of the element, the phases of each element are no longer aligned, and the superposition result is manifested as the decrease of peak sound pressure, the broadening of the main lobe, and the rise of side lobes. If $\Delta\phi\left(x_n\right)$ is regarded as a zero-mean phase perturbation with variance σ_{φ}^2, the array coherent gain can be approximately expressed as:

$$G \approx \exp\left(-\frac{\sigma_{\phi}^2}{2}\right). \tag{16}$$

Theoretical calculation proves that the geometric path difference ΔL caused by curved surface detection has a quadratic distribution relationship with position x, which will inevitably introduce exponential coherent gain loss. The smaller the curvature radius *R*, the more serious the phase distortion $\Delta\phi$, thus leading to severe wavefront broadening and energy divergence. Based on this, the experimental design will explore the limitations of different degrees of phase distortion on the bottom wave capture ability by comparing lead blocks without curvature, samples with fixed curvature, and actual lead seals with variable curvature.

Similarly, the curvature-related path-difference and coherence-loss analysis is based on several simplifying assumptions, such as the local arc approximation, the small-slope condition, homogeneous acoustic properties, and an idealized propagation path without fully considering coupling-layer fluctuation, three-dimensional beam spreading, or complex interfacial reflections. In actual lead-seal components, the inspected regions may differ not only in curvature, but also in material composition and interface structure. As a result, the experimentally observed variations in bottom-wave intensity and defect visibility may not be solely attributed to curvature. Therefore, the present theoretical analysis should be regarded as a simplified framework for interpreting the general influence trend of curvature on beam focusing and echo coherence, rather than a strict quantitative description of all propagation behaviors in real lead-seal assemblies.

3.3.2. Experimental testing and analysis

The surface of the lead seal is of variable curvature. Curved surface contact leads to uneven contact between the probe elements and the lead seal surface, and some elements may be suspended, resulting in a decrease in sound energy transmission efficiency. In addition, uneven coupling thickness is easy to occur in areas with large curvature, causing sound wave refraction, which will change the incident angle of the sound beam and lead to fluctuation of detection sensitivity. In this section, ultrasonic phased array testing is carried out on lead blocks without curvature, with fixed curvature, and lead seal specimens with variable curvature (profile at the highest point). Samples with different curvatures are shown in **Figure 16a–c**, and the detailed information of samples and defects is shown in **Figure 16d–f**.

(a) Lead block (no curvature).

(b) Lead block (fixed curvature).

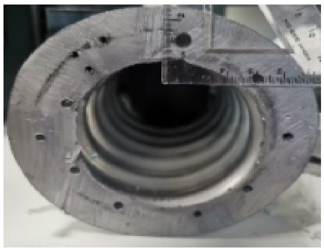

(c) Lead seal (variable curvature).

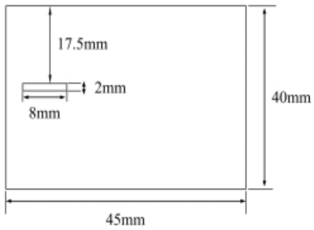

(d) Detailed defect information of the sample without curvature.

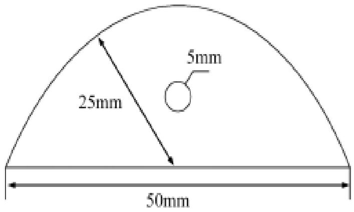

(e) Detailed defect information of the sample with fixed curvature.

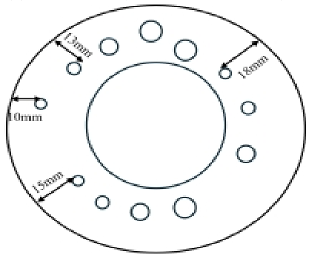

(f) Detailed defect information of the sample with variable curvature.

Figure 16. Plot of specimens with different curvatures.

As shown in **Figure 17**, by comparing the testing results of lead blocks without curvature, with fixed curvature, and lead seals with variable curvature, it is found that the ultrasonic phased array can effectively detect the internal defects of the three curvatures, but the bottom wave can be clearly seen in the lead block with or without defects, which is conducive to judging the defect information through the position of the bottom wave, while the bottom-wave response in the lead-seal specimen was less visible than that in the flat lead block under the same inspection settings. The bottom-wave amplitude appeared reduced in the variable-curvature region, and in some cases, the bottom-wave response was not clearly identifiable. This phenomenon can be explained by the phase distortion theory in Subsection 2.3.1: the variable curvature characteristic of the lead seal surface causes significant nonlinear time delay error $\Delta\phi$ of each element echo, leading to serious energy diffusion of the sound beam on the reflection path. Since the aluminum sheath at the bottom of the lead seal presents a wavy curved surface, the coherent gain decreases exponentially according to formula (16) under the action of double-curved surface scattering of the incident sound beam, thereby reducing the energy returned to the probe and lowering the visibility of the bottom-wave response. This experimental result is consistent with the derivation of imaging degradation caused by curvature in the theoretical model.

To better reflect practical inspection conditions, returned high-voltage cable terminal lead seals were selected in this section. In order to reduce the influence of surface roughness, all inspected regions were mechanically polished before testing, and no coupling device was used, so that roughness-related and coupling-related differences were minimized as much as possible under the present experimental conditions. However, it should be emphasized that the three inspected locations were not completely equivalent in all other aspects.

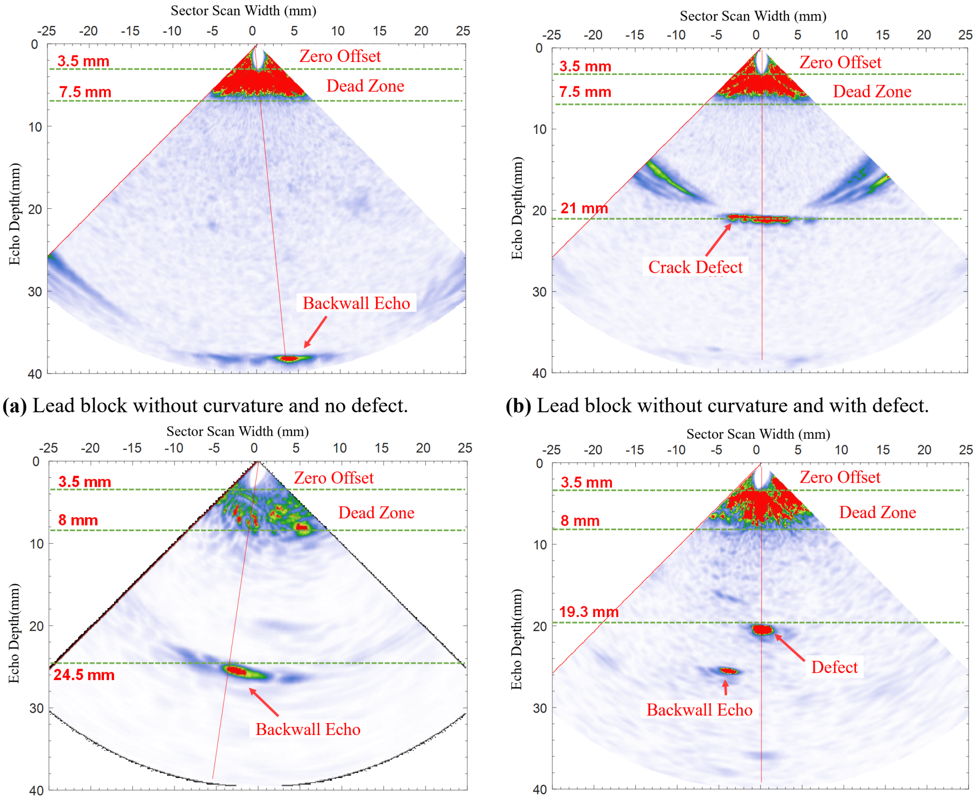

(a) Lead block without curvature and no defect.

(b) Lead block without curvature and with defect.

(c) Testing of a lead block with fixed curvature and no defect.

(d) Testing of a lead block with fixed curvature and with a defect.

(e) Testing of a lead seal with variable curvature and no defect.

(f) Testing of lead seals with variable curvature and with defects.

Figure 17. Detection results of samples with different curvatures.

The curvature characteristics of the three tested locations were defined as follows: the copper tail tube region had a relatively regular geometry and a nearly flat interface and was therefore treated as a low-curvature region; the highest point of the lead seal had the smallest local curvature radius and represented a high-curvature region; the aluminum sheath region exhibited a wavy bottom interface and was regarded as a complex variable-curvature region. The lead-seal samples are shown in **Figure 18a**,**b**, and the corresponding defect information is shown in **Figure 18c**.

Through comparison, it can be found that the bottom surfaces of the lead blocks were uniform planes, whereas the bottom surface of the tested lead seal was a wavy aluminum sheath. When ultrasonic waves interacted with the curved aluminum sheath, additional refraction and reflection occurred, reducing the observable bottom-wave response. In addition, when the upper surface curvature was large or when defects were present, further beam deflection could occur, which may further reduce the visibility of the bottom-wave signal. Under the present conditions, the bottom-wave response of the lead seal was less consistently observed than that of the lead block.

(a) Lead seal sample without defect.

(b) Lead seal sample with defect.

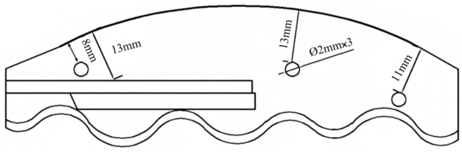

(c) Actual defect information of lead seal sample.

Figure 18. Samples of seals with different curvatures.

The testing results are shown in **Figure 19**. For the copper tail tube region, the bottom-wave response remained clearly visible in both defect-free and defective cases (**Figure 19a,b**), which is consistent with the relatively small curvature and the corresponding weak phase distortion. At the highest point of the lead seal, defect echoes were still identifiable, but the bottom-wave response became less clear (**Figure 19c,d**), which is consistent with the larger curvature and the stronger path-difference-induced phase distortion described in Subsection 3.3.1. In the aluminum sheath region, the bottom-wave response showed lower continuity and visibility (**Figure 19e,f**). This behavior may be related not only to curvature but also to the wavy multilayer interfacial structure of the aluminum sheath, which can independently affect ultrasonic propagation and reflection.

Therefore, although the present results suggest that curvature is closely associated with the degradation of bottom-wave response and imaging quality, the observed differences cannot be completely attributed to curvature alone. Material composition and interface structure are also potential influencing factors, particularly in the aluminum sheath region. Accordingly, the present experiment should be interpreted as demonstrating the combined effect of curvature-related geometry and local structural characteristics under realistic lead-seal conditions, rather than as a strictly isolated single-factor verification of curvature. More rigorously controlled specimens with identical material/interface conditions but different curvatures, or surface-compensation-based imaging analyses, are still required in future work to isolate the independent contribution of curvature.

Future work will require dedicated control specimens with identical material and interface conditions but different curvature radii, so that the independent influence of curvature can be evaluated more rigorously.

The testing results are shown in **Figure 19**, and the following conclusions can be drawn through comparison:

Copper tail tube: the testing results show that the bottom wave signal is clearly visible regardless of whether there is a defect (**Figure 19a**,**b**). This verifies that under the condition of small curvature, the phase distortion $\Delta\phi$ of the sound wave is extremely small, and the sound beam can maintain good coherence and realize concentrated reflection of energy.

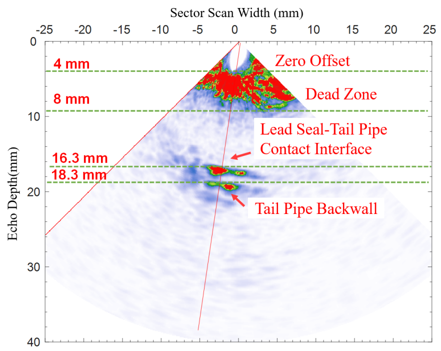

(a) No defect at the copper tail tube of the lead seal.

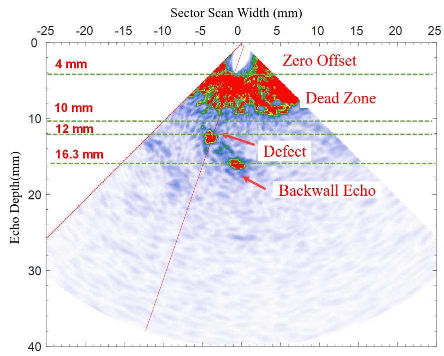

(b) With defect at the copper tail tube of the lead seal.

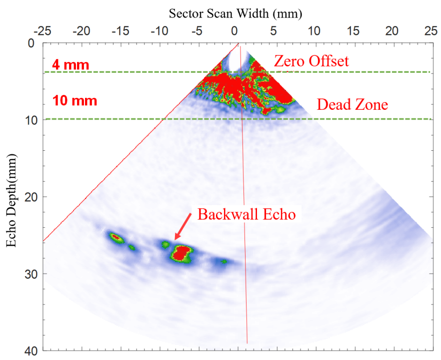

(c) No defect at the highest point of the lead seal.

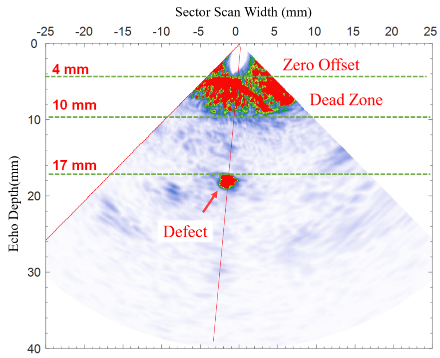

(d) With a defect at the highest point of the lead seal.

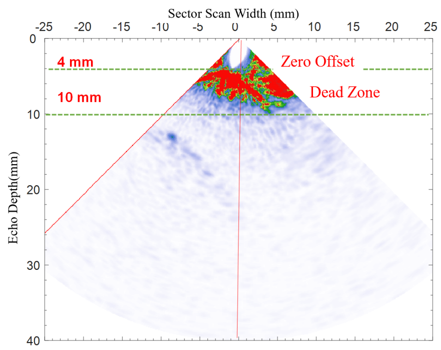

(e) No defect at the aluminum sheath of the lead seal.

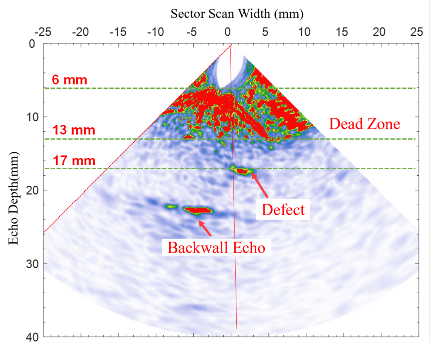

(f) With defect at the aluminum sheath of the lead seal.

Figure 19. Sample test results of seals with different curvatures.

The highest point of the lead seal: when testing here, the defect identification effect is significant, but the reception of the bottom wave signal is affected (**Figure 19c**,**d**). According to the theoretical analysis in Subsection 2.3.1, this is because the high curvature of the surface at this position leads to a severe quadratic distribution of the geometric path difference ΔL between elements, introducing serious phase distortion. This distortion destroys the focusing superposition condition of the sound beam in the far field, leading to serious energy diffusion of the sound wave on the reflection path, making the energy reflected back to the probe lower than the detection threshold.

Aluminum sheath: the testing results show that the bottom-wave response appeared less continuous and had a lower observable amplitude (**Figure 19e**,**f**). This phenomenon verifies that the wavy aluminum sheath interface at the bottom produces secondary scattering interference on the sound beam. Since the incident sound beam itself has been deflected by the influence of surface curvature, when it contacts the wavy curved surface, the refraction and reflection paths are further cluttered, resulting in extremely weak and unstable received bottom wave energy.

The experimental results suggest that surface curvature is an important contributing factor to imaging degradation and bottom-wave loss. However, the observed differences may also be influenced by variations in material composition and interface structure among the inspected regions. By eliminating the interference of roughness and coupling, this experiment proves the corresponding relationship between the curvature radius R and the coherent gain loss in the theoretical derivation.

4. Conclusion

This paper focuses on the influence of coupling state, surface roughness, and interface curvature on the imaging quality of phased array ultrasound and analyzes its action mechanism. The main conclusions are as follows.

(1) From a mechanistic perspective, the results suggest that surface roughness and surface curvature are important factors associated with imaging degradation under the investigated conditions. Increased surface roughness may enhance diffuse reflection and reduce the effective coherent energy among array elements, whereas variable surface curvature may introduce spatial phase deviation in the received echoes, thereby weakening coherent superposition at the preset focal region. These effects are generally reflected in reduced sound-pressure concentration, mainlobe broadening, and less distinct defect boundaries in the reconstructed images. It should be noted, however, that the roughness- and curvature-related analyses in this study were based on simplified theoretical assumptions and are therefore mainly intended to explain the observed trends rather than to provide a fully quantitative description of wave propagation in real lead-seal structures.

(2) From an engineering perspective, the proposed flexible film coupling device showed better coupling conformity and imaging performance than the conventional rigid wedge under the tested conditions. In addition, comparative observations at different inspected regions, including the copper tail tube, the highest point of the lead seal, and the aluminum sheath, indicate that changes in local geometry are closely associated with variations in imaging response and bottom-wave visibility. However, these regional differences may also be influenced by local material composition and interface structure, especially in the aluminum sheath region with a wavy multilayer interface. Therefore, the present results should be interpreted as demonstrating the combined influence of geometric and structural factors under realistic lead-seal conditions, rather than the independent effect of curvature alone.

Overall, the study provides experimental evidence and practical reference for understanding the factors that affect phased array ultrasonic inspection of lead-seal defects, while more rigorously controlled specimens and dedicated quantitative validation are still needed in future work.

Author contributions: Conceptualization, PH and JC; methodology, PH and FZ; software, LW; validation, PH, JC and CQ; formal analysis, FZ; investigation, JC, LW and CQ; resources, PH; data curation, FZ; writing—original draft preparation, JC; writing—review and editing, PH; visualization, LW; supervision, PH; project administration, PH; funding acquisition, PH. All authors have read and agreed to the published version of the manuscript.

Funding: This work received no external funding.

Institutional review board statement: Not applicable.

Informed consent statement: Not applicable.

Data availability statement: The data that support the findings of this study are available from the corresponding author upon reasonable request

Conflict of interest: The authors declare no conflict of interest.

AI use statement: The authors declare that no artificial intelligence (AI) tools were used in the preparation of this manuscript.

References

1. Fang CH, Hu JZ, Tao YN, et al. Ultrasonic phased array flexible coupling detection of defects in high-voltage cable termination seals. High Voltage Technology. 2022; 48(1): 29–37. (in Chinese)
2. Fang CH, Zhou G, Rao D, et al. Quantitative ultrasonic detection of sealing defects in high-voltage cable accessories. Journal of Electronic Measurement and Instrumentation. 2024; 38(6): 125–134. (in Chinese)
3. Cao JP, Wang SH, Ren GZ, et al. Experimental validation and application of eddy current flaw detection method for lead seals of high voltage cable accessories. High Voltage Technology. 2018; 44(11): 3720–3726. (in Chinese)
4. Wu ZR, Wu JT, Li ZJ. Fault diagnosis method of cable terminal grounding system based on metal sheath current and voltage. Electrotechnology. 2025; (3): 138–141,145. (in Chinese)
5. Fang CH, Zhou G, Shao B, et al. Ultrasonic image convolutional neural network identification of defects in high-voltage cable terminal seals. Applied Acoustics. 2025; 44(1): 80–87. (in Chinese)
6. Zhang J, Drinkwater B, Wilcox P. Effect of roughness on imaging and sizing rough crack-like defects using ultrasonic arrays. IEEE Transactions on Ultrasonics, Ferroelectrics and Frequency Control. 2012; 59(5): 939–948. doi: 10.1109/TUFFC.2012.2278
7. McKee JG, Wilcox PD, Malkin RE. Effect of surface compensation for imaging through doubly-curved surfaces using a 2D phased array. In: Proceedings of the 45th Annual Review of Progress in Quantitative Nondestructive Evaluation; 5–19 July 2018; Burlington, VT, USA. p. 100008. doi: 10.1063/1.5099836
8. Rodrigues Filho JFM, Bélanger P. Probe Standoff Optimization Method for Phased Array Ultrasonic TFM Imaging of Curved Parts. Sensors. 2021; 21(19): 6665. doi: 10.3390/s21196665.
9. Drinkwater BW, Wilcox PD. Ultrasonic arrays for non-destructive evaluation: A review. NDT & E International. 2006; 39(7): 525–541. doi: 10.1016/j.ndteint.2006.03.006
10. Holmes C, Drinkwater BW, Wilcox PD. Post-processing of the full matrix of ultrasonic transmit–receive array data for non-destructive evaluation. NDT & E International. 2005; 38(8): 701–711. doi: 10.1016/j.ndteint.2005.04.002
11. Mahaut S, Roy O, Beroni C, et al. Development of phased array techniques to improve characterization of defect located in a component of complex geometry. Ultrasonics. 2002; 40(1–8): 165–169. doi: 10.1016/S0041-624X(02)00131-2

12. Sun X, Drinkwater BW, Croxford AJ. Continuous monitoring with a permanently installed high-resolution ultrasonic phased array. Structural Health Monitoring. 2023; 22(5): 3451–3464. doi: 10.1177/14759217231152413.
13. Lei X, Wirdelius H, Rosell A. Simulation-Based Investigation of a Probability of Detection (POD) Model Using Phased Array Ultrasonic Testing (PAUT) Technique. Journal of Nondestructive Evaluation. 2022; 41(2): 40. doi: 10.1007/s10921-022-00873-2.
14. Hunter AJ, Drinkwater BW, Wilcox PD. Autofocusing ultrasonic imagery for non-destructive testing and evaluation of specimens with complicated geometries. NDT & E International. 2010; 43(2): 78–85. doi: 10.1016/j.ndteint.2009.09.001
15. Huggett DJ, Dewan MW, Wahab MA, et al. Phased Array Ultrasonic Testing for Post-Weld and OnLine Detection of Friction Stir Welding Defects. Research in Nondestructive Evaluation. 2017; 28(4): 187–210. doi: 10.1080/09349847.2016.1157660
16. Chatillon S, Cattiaux G, Serre M, et al. Ultrasonic non-destructive testing of pieces of complex geometry with a flexible phased array transducer. Ultrasonics. 2000; 38(1–8): 131–134. doi: 10.1016/S0041-624X(99)00181-X
17. Schmerr LW. Fundamentals of Ultrasonic Nondestructive Evaluation. Springer; 2016.
18. Nicolson E, Mohseni E, Lines D, Tant KMM, Pierce G, MacLeod CN. Towards an in-process ultrasonic phased array inspection method for narrow-gap welds. NDT & E International. 2024; 144: 103074. doi: 10.1016/j.ndteint.2024.103074.
19. Yamada T, Ohara Y, Ulrich TJ, et al. High-resolution 3D ultrasonic imaging using high-frequency piezoelectric transmitter and ultra-multiple laser 2D scanning. NDT & E International. 2024; 146: 103178. doi: 10.1016/j.ndteint.2024.103178
20. Prada C, Thomas JL, Fink M. The iterative time reversal process: Analysis of the convergence. The Journal of the Acoustical Society of America. 1995; 97(1): 62–71. doi: 10.1121/1.412285
21. Wilcox P, Lowe M, Cawley P. The effect of dispersion on long-range inspection using ultrasonic guided waves. NDT & E International. 2001; 34(1): 1–9. doi: 10.1016/S0963-8695(00)00024-4
22. Lowe MJS, Cawley P, Kao JY, et al. The low frequency reflection characteristics of the fundamental antisymmetric Lamb wave a_0 from a rectangular notch in a plate. The Journal of the Acoustical Society of America. 2002; 112(6): 2612–2622. doi: 10.1121/1.1512702
23. Rose JL. Ultrasonic Waves in Solid Media. Cambridge University Press; 2014.
24. Krautkrämer J, Krautkrämer H. Ultrasonic Testing of Materials. Springer-Verlag; 1990.
25. Saini A, Lane CJL, Tu J, et al. 3D ultrasonic imaging of surface-breaking cracks using a linear array. Ultrasonics. 2022; 125: 106790. doi: 10.1016/j.ultras.2022.106790
26. Silk MG. Ultrasonic Transducers for Nondestructive Testing. Adam Hilger; 1984.